Polymer ultrapermeability from the inefficient packing of 2D chains

Polymer Ultrapermeability from the Inefficient Packing of 2D Chains

Ian Rose[1], C. Grazia Bezzu[1], Mariolino Carta[1], Bibiana Comesaña-Gándara[1], Elsa Lasseuguette[2], M. Chiara Ferrari[2], Paola Bernardo[3], Gabriele Clarizia[3], Alessio Fuoco[3], Johannes C. Jansen[3], Kyle E. Hart,[4] Thilanga P. Liyana-Arachchi[5], Coray M. Colina[5], Neil B. McKeown[1]*

[1]EastChem, School of Chemistry, The University of Edinburgh, David Brewster Road, Edinburgh, EH9 3FJ, UK.

[2]School of Engineering, The University of Edinburgh, Robert Stevenson Road, Edinburgh, EH9 3FB, UK.

[3]Institute on Membrane Technology, ITM-CNR, c/o University of Calabria, Via P. Bucci 17/C, 87036 Rende (CS), Italy.

[4]Department of Materials Science and Engineering, The Pennsylvania State University, University Park, PA 16802, USA.

[5]Department of Chemistry, The University of Florida, 318 Leigh Hall, P.O. Box 117200, Gainesville, FL 32611-7200, USA.

*Correspondence to: Prof. Neil B. McKeown, EastChem, School of Chemistry, The University of Edinburgh, David Brewster Road, EH9 3FJ, UK; email: neil.mckeown@ed.ac.uk

The promise of ultrapermeable polymers, such as poly(trimethylsilylpropyne) (PTMSP), for reducing the size and increasing the efficiency of membranes for gas separations remains unfulfilled due to their poor selectivity. We report an ultrapermeable polymer of intrinsic microporosity (PIM-TMN-Trip) that is substantially more selective than PTMSP. From molecular simulations and experimental measurement we find that the inefficient packing of the 2D chains of PIM-TMN-Trip generates a high concentration of both small (< 0.7 nm) and large (0.7-1.0 nm) micropores, the former enhancing selectivity and the latter permeability. Gas permeability data for PIM-TMN-Trip surpass the 2008 Robeson upper bounds for O_2/N_2, H_2/N_2, CO_2/N_2, H_2/CH_4 and CO_2/CH_4, with the potential for biogas purification and carbon capture demonstrated for relevant gas mixtures. Comparisons between PIM-TMN-Trip and structurally similar polymers with 3D contorted chains confirm that its additional intrinsic microporosity is generated from the awkward packing of its 2D polymer chains in a 3D amorphous solid. This strategy of shape-directed packing of chains of microporous polymers may be applied to other rigid polymers for gas separations.

Increasing the permeability of polymers used for gas separation membranes is desirable to enhance productivity and reduce the size of membranes required for large-scale gas and vapor separations. These applications include natural gas upgrading, nitrogen or oxygen separation from air, and the capture of carbon dioxide.[1-5] To date, only a few polyacetylenes demonstrate *ultrapermeability*, as best exemplified by the extensively studied poly(trimethylsilylpropyne) (PTMSP; Supplementary Fig. 1), which has been recognized as the most permeable polymer since it was first reported in 1983.[6] PTMSP and the other structurally related ultrapermeable polyacetylenes[7,8] possess rigid and contorted macromolecular chains with low inter-chain cohesive energy resulting in space inefficient packing. The resulting glassy solids possess large (> 0.5 nm) and highly interconnected voids that facilitate rapid gas transport.[9] However, the practical use of these ultrapermeable polyacetylenes as gas separation membranes is prohibited by very low selectivity for the separation of one gas over another (Supplementary Table 1). More recently, Polymers of Intrinsic Microporosity (e.g. PIM-1; Supplementary Fig. 1), which are also comprised of 3D contorted macromolecular structures, have been investigated as materials for gas separation membranes.[10-13] PIMs demonstrate higher selectivity than PTMSP for the separation of some important gas pairs (e.g. O_2/N_2; H_2/N_2; CO_2/N_2; CO_2/CH_4), due to their greater chain rigidity and stronger inter-chain cohesive interactions. However, despite recent advances,[14,15] no PIM has yet approached the exceptionally high gas permeability demonstrated by PTMSP (Supplementary Table 1).

Polymer design, simulation and synthesis

PIMs derived from bridged bicyclic components such as triptycene (e.g. TPIM-1 and PIM-Trip-TB; Supplementary Fig. 1) have recently provided a large step-change in gas selectivity – an enhancement attributable to their rigid structures.[16-20] Triptycene's three-fold symmetry also makes it an excellent building block for the assembly of honeycomb-like two-dimensional (2D) porous polymers, both crystalline[21-23] and amorphous[24-26], which in principle, could act as efficient molecular sieve membranes.[27] However, despite many elegant synthetic approaches to 2D porous polymers,[28-30] none are suitable for membrane applications due to the insolubility of their extended network structures. Therefore, a polymer composed of discrete 2D macromolecular chains that can be processed from solution into robust films or large-area

coatings is an attractive target for synthesis. Our structural design for such a 2D polymer includes: (a) triptycene units fused together via dibenzodioxin linking groups to ensure that each triptycene is co-planar to its neighbor in 2D ribbon-shaped chains[26] but linked via only two of the three phenyl rings of triptycene to prohibit network formation; and (b) an extended substituent fused to the remaining triptycene phenyl ring to enhance 2D aspect ratio. Independent molecular simulations of the amorphous solid-state packing reinforced the intuitive predictions that such rigid 2D polymer chains pack inefficiently so as to form large interconnected pores suitable for enhanced gas permeability (Methods, Supplementary Information).

The target 2D ribbon-shaped polymer, PIM-TMN-Trip (Fig. 1), was constructed using a monomer based on triptycene that contains a fused tetramethyltetrahydronaphthalene (TMN) unit as the extended substituent (Methods, Supplementary Scheme 1 and Supplementary information).[31] This bulky substituent imparts solubility in organic solvents as demonstrated by comparison with the structurally related 2D polymer, PIM-BTrip, which proved insoluble in all organic solvents (Supplementary Scheme 2 and Supplementary Information). The greater BET surface area (SA_{BET}) of PIM-TMN-Trip (1050 m^2 g^{-1}) relative to PIM-BTrip (791 m^2 g^{-1}), as calculated from N_2 adsorption data (Fig. 2 and Supplementary Fig. 6), indicates that the greater 2D aspect ratio provided by the TMN substituents generates enhanced intrinsic microporosity.

In order to compare the 2D PIM-TMN-Trip with a structurally similar polymer, which contains the extended TMN substituents but with chains contorted in three-dimensions, PIM-TMN-SBI was prepared. PIM-TMN-SBI is analogous to the much-studied PIM-1 but with two extended TMN units fused to each of its spirobisindane (SBI) units. The required TMN-Trip and TMN-SBI monomers were both prepared via a multi-step synthesis (Supplementary Scheme 1) and their structures confirmed by spectroscopy and single crystal x-ray analysis (Supplementary Figs. 2 and 4). Successful polymerization of the appropriate monomer with tetrafluoroterephthalonitrile was achieved using the dibenzodioxin-forming polymerization reaction that was developed originally to make PIM-1.[10] Both polymers proved soluble in chloroform, which allowed structural characterization, using Nuclear Magnetic Resonance (NMR) spectroscopy and Gel Permeation Chromatography (GPC, Supplementary Figs. 3 and 5). Robust free-standing films, suitable for gas permeability measurements, were prepared by simple casting from solution. Macromolecular packing models (~9 × 9 × 9 nm) of PIM-TMN-Trip and PIM-TMN-SBI were constructed using the *Polymatic* simulated polymerization algorithm[32] and

the '21-step' compression/decompression scheme which has been successfully applied to model other PIMs (Methods and Supplementary Information).[33]

Physical characterization

Structure analysis of PIM-TMN-Trip and PIM-TMN-SBI was performed using gas adsorption and wide-angle x-ray scattering (WAXS) and the resulting data were compared to those calculated from the computational models. Nitrogen adsorption analysis of powdered samples at 77 K demonstrates uptake at low pressure indicating freely accessible microporosity (Fig. 2a). The nitrogen isotherms provided apparent SA_{BET} of 1050 for PIM-TMN-Trip and 1015 m^2 g^{-1} for PIM-TMN-SBI, which are remarkably close to the predicted SA_{BET} values of 1110 and 1050 m^2 g^{-1} calculated from the respective macromolecular packing simulations.

The greater CO_2 adsorption at 273 K/1 bar of 3.3 mmol g^{-1} for PIM-TMN-Trip in comparison to 2.5 mmol g^{-1} for PIM-TMN-SBI (Fig. 2b) suggests that the former has a larger number of accessible pores in the ultramicroporous range (i.e. of diameter < 0.7 nm), which are associated with enhanced gas selectivity.[20] The high CO_2 uptake of PIM-TMN-Trip contrasts greatly with that of poorly selective PTMSP (1 mmol g^{-1}).[34] The greater ultramicroporosity of PIM-TMN-Trip was confirmed by pore size distribution (PSD) analysis of low-pressure N_2 adsorption data using the Horvath-Kawazoe (HK) model, assuming carbon slit-pore geometry (Fig. 2c).[11] Importantly, PSD calculated from both HK analysis of gas adsorption data and from molecular simulations indicate that PIM-TMN-Trip also has a much higher proportion of larger micropores (0.7-1.0 nm) than PIM-TMN-SBI.

WAXS confirms the amorphous nature of both PIM-TMN-Trip and PIM-TMN-SBI, although the different positions of the pronounced halos, arising from inter- and intra-chain structural correlations, indicate that the space-efficiency of the packing of the 2D and 3D chains are different (Fig. 2d). For PIM-TMN-Trip the two main diffuse halos are at smaller values of 2θ corresponding to larger structural correlations (2.2-3.5 nm and ~0.80 nm), suggesting a less dense packing of the polymer chains relative to those of PIM-TMN-SBI (1.3-1.8 nm and ~0.70 nm). Importantly, WAXS data calculated from the models of both PIM-TMN-Trip and PIM-TMN-SBI are similar to those obtained by measurement from films, which validates the molecular simulations (Fig. 2d). The simulations show that PIM-TMN-Trip has a fractional free volume (FFV) of 0.309 ± 0.005, which is very similar to the experimental value of 0.314 ± 0.005

derived from a methanol treated film (of density = 0.965±0.002 g cm^{-3}) and is greater than the free volume calculated for PIM-TMN-SBI (0.276±0.004).

Tensile tests on 5 mm wide strips of methanol treated films of PIM-TMN-Trip gave a value for the Young's modulus of 1.31±0.07 GPa, tensile strength of 55.5±2.6 MPa and a maximum strain of 12.9±4.3% (Supplemental Fig. 9). These values compare favourable to those of other PIMs,[14] therefore, the 2D chain structure gives PIM-TMN-Trip very high rigidity, without making it excessively brittle, which would prohibit fabrication of gas separation membranes. The mechanical robustness of PIM-TMN-Trip films implies significant polymer chain entanglement as observed in the chain-packing simulations.

Gas Permeability

Films of PIM-TMN-Trip demonstrate exceptionally high values of gas permeability (Table 1). However, the evaluation of gas permeability data for a new polymer requires careful consideration of film history prior to measurement, as a great disparity in values are often reported for the same polymer. Generally, the highest reported values of gas permeability for polyacetylenes and PIMs were measured from films freshly treated with methanol (Supplementary Table 1). Such treatment is known to remove any residual casting solvent and induces additional free volume.[11] A film of PIM-TMN-Trip, measured 24 h after methanol treatment, is approximately twice as gas permeable as PIM-TMN-SBI, despite the latter being as permeable as any PIM reported to date (Table 1 and Supplementary Table 1).[14,15] The values for methanol treated PIM-TMN-Trip and PIM-TMN-SBI are in reasonable agreement with those calculated from the packing models (Table 1). Importantly, the gas permeabilities of methanol treated PIM-TMN-Trip are within the range reported for methanol treated PTMSP (e.g. P_{CO_2} = 28-47 × 10^3 Barrer).[7,35-37]

Variability in film history means that the most informative method of demonstrating the potential of a novel polymer for the separation of a particular gas pair (x and y) is to place its permeability data on a Robeson plot (i.e. log P_x *vs.* log P_x/P_y) to assess its position relative to the benchmark upper bound.[38] Fig. 3 shows the Robeson plots for the O_2/N_2, H_2/N_2, CO_2/N_2 and CO_2/CH_4 gas pairs containing data for PIM-TMN-Trip and PIM-TMN-SBI, obtained from films with a variety of processing histories and periods of ageing, together with accumulated data for PTMSP, other highly permeable polyacetylenes, PIM-1 and other PIMs. The exceptional values

for gas permeability combined with high selectively means that data for PIM-TMN-Trip are placed in previously unpopulated areas of the Robeson plots for all gas pairs and well above the 2008 upper bounds for O_2/N_2, H_2/N_2, H_2/CH_4, CO_2/N_2 and CO_2/CH_4 (Fig. 3).

For the O_2/N_2 and H_2/N_2 Robeson plots (Fig. 3a and b), the data points fall into three distinct groups, which are differentiated by the relative ability of the polymers to act as molecular sieves. Firstly, PTMSP and other polyacetylenes demonstrate very low selectivity across the full range of permeability resulting in their data falling below the 1991 upper bounds. Secondly, spirobisindane-based PIMs demonstrate both moderate selectivity and permeability, with data typically between the 1991 and 2008 upper bounds. Thirdly, triptycene-based PIMs and those derived from other bridged bicyclic units demonstrate moderate permeability but much enhanced selectivity due to their greater rigidity and improved molecular sieving properties, which has prompted the recent suggestion (2015) to again raise the upper bound for these gas pairs.[20] The data for the ultrapermeable PIM-TMN-Trip are clearly consistent with those of these high performing molecular-sieving polymers in which transport is dominated by diffusivity selectivity (Supplementary Table 3 and Supplementary Fig. 10).

The data for PIM-TMN-Trip are also positioned in an unpopulated region of both the CO_2/N_2 and CO_2/CH_4 Robeson plots (Fig. 3c and d), above the 2008 upper bounds and with greater values for selectivity than those of the ultrapermeable polyacetylenes. For these gas pairs the high solubility of CO_2 within PIM-TMN-Trip, as demonstrated by its adsorption isotherm (Fig. 2b), predominately enhances selectivity rather than a pure molecular sieving effect.

In contrast, the gas permeability data for PIM-TMN-SBI (Table 1 and Fig. 3) are close to the 2008 upper bounds on the Robeson plots in positions that are typical for previously reported PIMs based on spirobisindane units. Despite being much less permeable than PIM-TMN-Trip, the bulky TMN substituents enhance the gas permeability of PIM-TMN-SBI relative to PIM-1. The direct comparison of the gas permeability results of PIM-TMN-Trip and PIM-TMN-SBI confirms the conclusions from packing simulations that the 2D ribbon shape of PIM-TMN-Trip is responsible for inducing ultrapermeability.

Further confirmation of the importance of the 2D chain structure was obtained from a preliminary investigation of the properties of the novel polymer, PIM-TMN-Trip-TB, within which the TMN-triptycene units are linked together using Tröger's base (Supplementary Scheme

3 and Supplementary Fig. 1). PIM-TMN-Trip-TB is contorted in 3D due to the structure of the Tröger's base linking group.[14] In its methanol treated state, a film of PIM-TMN-Trip-TB demonstrates the typical gas permeability performance of a triptycene-based PIM with good selectivity for O_2/N_2 and H_2/N_2 but only moderate permeabilities (data point 10 on Table 1 and Fig. 3) relative to PIM-TMN-Trip. This result is complementary to that obtained from PIM-TMN-SBI for which the sites of 3D contortion within the polymer chain are the SBI monomeric units whereas for PIM-TMN-Trip-TB they arise from the TB linking groups. Therefore, despite 3D PIM-TMN-Trip-TB being composed of the same TMN-Trip monomeric component and 3D PIM-TMN-SBI possessing the same extended TMN substituents and dibenzodioxin linking group, only 2D PIM-TMN-Trip demonstrates ultrapermeability.

Gas permeability of methanol treated films of all highly permeable glassy polymers decreases on ageing due to the loss of induced free volume (Supplementary Table 1). Such ageing is apparent for PIM-TMN-Trip after 365 days (Table 1 and Supplementary Fig. 11), with reductions in gas permeability ranging from 24% (He) to 75% (CH_4). Notably, He permeability after aging is still higher than for any previously reported PIM in its freshly methanol treated state (Table 1 and Supplementary Table 1). Ageing provides a strong enhancement of selectivity so that the data for the year-old film is found at a desirable position of the Robeson plot for all important gas pairs with the data for O_2/N_2 approaching the recently proposed 2015 upperbound (Fig. 3a).[20] Hence, performance was assessed for this film using gas mixtures that mimic biogas (CO_2/CH_4; ~50/50) and flue gas ($N_2/O_2/CO_2$; 79.9/10.1/10.0). An excellent combination of high permeability ($P_{CO_2} > 10.0 \times 10^3$ Barrer) and selectivity ($P_{CO_2}/P_{N_2} > 19$; $P_{CO_2}/P_{CH_4} > 13$) was demonstrated, even at elevated feed pressures (6 bar), showing the potential of PIM-TMN-Trip for biogas purification and post-combustion carbon capture (Supplementary Tables 9 and 10). Physical ageing of polymers is much more rapid in thin films, for example, a recently reported study on PIM-1 hollow fibres[39] estimates that the gas permeability and selectivity of a freshly prepared thin (~3 μm) selective layer (e.g., P_{O_2} = 200 Barrer; P_{O_2}/P_{N_2} = 4.6) is similar to that of a thick film (102 μm) that had been aged for 1380 days.[40] The gas permeabilities for a thick film of PIM-TMN-Trip aged over 365 days suggest that it ages at a similar rate to PIM-1 (Supplementary Fig. 11), therefore, thin films of PIM-TMN-Trip may demonstrate further enhanced gas selectivity.

It is of interest to compare the properties of PIM-TMN-Trip with those of PTMSP, which is the archetypal ultrapermeable polymer and has been the subject of numerous reports and patents.[41] Both PIM-TMN-Trip and PTMSP possess a large amount of interconnected micropores of diameter in the range 0.6-1.0 nm, which facilitate rapid gas transport. However, PIM-TMN-Trip also possesses a large amount of smaller pores (<0.6 nm) relative to PTMSP (Fig. 2c).[12] These smaller micropores provide enhanced performance as a molecular sieve, which is apparent from the steeper correlation of the diffusion coefficient versus the effective gas diameter, especially for the 365 day aged film (Supplementary Fig. 10). It has been reported that heating of PTMSP results in the collapse of its metastable ultrapermeable phase at 80-100 °C.[42] In contrast, PIMs are routinely heated at 120-140 °C in a vacuum oven to remove the induced free volume following methanol treatment.[18] Surprisingly, no reduction in gas permeability was observed for methanol treated films of PIM-TMN-Trip following heating at 140 °C (data point 6, Table 1 and Fig. 3) in marked contrast to the drastic loss of permeability of PIM-TMN-SBI (~80%, data point 9, Table 1 and Fig. 3) or that reported for PTMSP on heating (~90%).[37,43-45] The permeability of H_2, N_2 and CO_2 through PIM-TMN-Trip measured at 100 °C (Table 1), and even above 200 °C ($P_{N_2} = 3.5 \times 10^3$ Barrer at 215 °C), also demonstrates that the ultrapermeable state of PIM-TMN-Trip is thermally stable in contrast to that of PTMSP.[42] Maintaining ultrapermeability at elevated temperatures may be of importance to a number of membrane applications including the use of contact membranes for the release of CO_2 from aqueous solvent in carbon capture systems which is performed at ~100 °C. Membranes of PTMSP have been evaluated for this application but provided relatively low permeance, presumably due to the thermal collapse of its pore structure.[46,47] PIM-TMN-Trip may also be suitable for other membrane applications proposed previously for PTMSP. These include hydrocarbon vapor separations, for which pore-blocking by larger molecules (e.g. butane) enhances selectivity over smaller molecules (e.g. H_2 or CH_4)[48,49], or the separation of alcohol biofuels from aqueous solutions using pervaporation.[50]

Outlook

The concept of 2D chain disrupted packing to enhance intrinsic microporosity extends the potential of polymer ultrapermeability beyond unselective polyacetylenes towards applications that require a more size-selective and robust pore structure. Ultimately, for industrial membrane applications of polymers such as PIM-TMN-Trip, fabrication into thin selective layers in the form of a thin film composite membrane or a hollow fibre is required to optimize permeance.

Although ultrapermeability will be lost through rapid ageing in such thin films, the graceful ageing of PIM-TMN-Trip over 1 year with commensurate increases in selectivities, suggests that the selectivities for separation of important gas pairs would approach those of commercial polymer membranes but with far greater permeances. This would allow significant reductions to the size of current membrane systems.

References

1 Baker, R. W. & Low, B. T. Gas separation membrane materials: A perspective. *Macromolecules* **47**, 6999-7013, (2014).

2 Bernardo, P., Drioli, E. & Golemme, G. Membrane gas separation: A review/state of the art. *Ind. Eng. Chem. Res.* **48**, 4638-4663, (2009).

3 Du, N. Y., Park, H. B., Dal-Cin, M. M. & Guiver, M. D. Advances in high permeability polymeric membrane materials for CO2 separations. *Energy Envron. Sci.* **5**, 7306-7322, (2012).

4 Budd, P. M. & McKeown, N. B. Highly permeable polymers for gas separation membranes. *Polym. Chem* **1**, 63-68, (2010).

5 Wang, S. F. *et al.* Advances in high permeability polymer-based membrane materials for CO2 separations. *Energy Envron. Sci.***9**, 1863-1890, (2016).

6 Masuda, T., Isobe, E., Higashimura, T. & Takada, K. Poly 1-(trimethylsilyl)-1-propyne - a new high polymer synthesized with transition-metal catalysts and characterized by extremely high gas-permeability. *J. Am. Chem. Soc.* **105**, 7473-7474, (1983).

7 Hu, Y., Shiotsuki, M., Sanda, F., Freeman, B. D. & Masuda, T. Synthesis and properties of indan-based polyacetylenes that feature the highest gas permeability among all the existing polymers. *Macromolecules* **41**, 8525-8532, (2008).

8 Shiotsuki, M., Sanda, F. & Masuda, T. Polymerization of substituted acetylenes and features of the formed polymers. *Polym. Chem* **2**, 1044-1058, (2011).

9 Wang, X.-Y., Hill, A. J., Freeman, B. D. & Sanchez, I. C. Structural, sorption and transport characteristics of an ultrapermeable polymer. *J. Membr. Sci.* **314**, 15-23, (2008).

10 Budd, P. M. *et al.* Polymers of intrinsic microporosity (PIMs): robust, solution- processable, organic nanoporous materials. *Chem. Commun.*, 230-231, (2004).

11 Budd, P. M. *et al.* Gas permeation parameters and other physicochemical properties of a polymer of intrinsic microporosity: Polybenzodioxane PIM-1. *J. Membr. Sci.* **325**, 851-860, (2008).

12 Budd, P. M. *et al.* Gas separation membranes from polymers of intrinsic microporosity. *J. Membr. Sci.* **251**, 263-269, (2005).

13 Kim, S. & Lee, Y. M. Rigid and microporous polymers for gas separation membranes. *Prog. Polym. Sci.* **43**, 1-32, (2015).

14 Rose, I. *et al.* Highly Permeable Benzotriptycene-Based Polymer of Intrinsic Microporosity. *ACS Macro Lett.* **4**, 912-915, (2015).

15 Zhang, J. *et al.* The enhancement of chain rigidity and gas transport performance of polymers of intrinsic microporosity via intramolecular locking of the spiro-carbon. *Chem. Commun.* **52**, 6553-6556, (2016).

16 Carta, M. *et al.* Triptycene Induced Enhancement of Membrane Gas Selectivity for Microporous Troger's Base Polymers. *Adv. Mater.* **26**, 3526-3531, (2014).

17 Ghanem, B. S., Swaidan, R., Litwiller, E. & Pinnau, I. Ultra-microporous triptycene-based polyimide membranes for high-performance gas separation. *Adv. Mater.* **26**, 3688-3692, (2014).

18 Ghanem, B. S., Swaidan, R., Ma, X. H., Litwiller, E. & Pinnau, I. Energy-efficient hydrogen separation by ab-type ladder-polymer molecular sieves. *Adv. Mater.* **26**, 6696-6700, (2014).

19 Carta, M. *et al.* An Efficient Polymer Molecular Sieve for Membrane Gas Separations. *Science* **339**, 303-307, (2013).

20 Swaidan, R., Ghanem, B. & Pinnau, I. Fine-Tuned Intrinsically Ultramicroporous Polymers Redefine the Permeability/Selectivity Upper Bounds of Membrane-Based Air and Hydrogen Separations. *ACS Macro Lett.* **4**, 947-951, (2015).

21 Kahveci, Z., Islamoglu, T., Shar, G. A., Ding, R. & El-Kaderi, H. M. Targeted synthesis of a mesoporous triptycene-derived covalent organic framework. *CrystEngComm* **15**, 1524-1527, (2013).

22 Kissel, P., Murray, D. J., Wulftange, W. J., Catalano, V. J. & King, B. T. A nanoporous two-dimensional polymer by single-crystal-to-single-crystal photopolymerization. *Nature Chem.* **6**, 774-778, (2014).

23 Murray, D. J. *et al.* Large area synthesis of a nanoporous two-dimensional polymer at the air/water interface. *J. Am. Chem. Soc.* **137**, 3450-3453, (2015).

24 Ghanem, B. *et al.* A triptycene-based polymer of intrinsic microposity that displays enhanced surface area and hydrogen adsorption. *Chem. Commun.*, 67-69, (2007).

25 Ghanem, B. S. *et al.* Triptycene-based polymers of intrinsic microporosity: organic materials that can be tailored for gas adsorption. *Macromolecules* **43**, 5287-5294, (2010).

26 Thomas, S. W. *et al.* Perpendicular organization of macromolecules: Synthesis and alignment studies of a soluble poly(iptycene). *J. Am. Chem. Soc.* **127**, 17976-17977, (2005).

27 Zang, Y. *et al.* Two-dimensional and related polymers: Concepts, synthesis, and their potential application as separation membrane materials. *Polym. Rev.* **55**, 57-89, (2015).

28 Colson, J. W. & Dichtel, W. R. Rationally synthesized two-dimensional polymers. *Nature Chem.* **5**, 453-465, (2013).

29 Payamyar, P., King, B. T., Ottinger, H. C. & Schluter, A. D. Two-dimensional polymers: concepts and perspectives. *Chem. Commun.* **52**, 18-34, (2016).

30 Zhuang, X., Mai, Y., Wu, D., Zhang, F. & Feng, X. Two-dimensional soft nanomaterials: A fascinating world of materials. *Adv. Mater.* **27**, 403-427, (2015).

31 Taylor, R. G. D. *et al.* The Synthesis of Organic Molecules of Intrinsic Microporosity Designed to Frustrate Efficient Molecular Packing. *Chem. Eur. J.* **22**, 2466-2472, (2016).

32 Abbott, L. J., Hart, K. E. & Colina, C. M. Polymatic: a generalized simulated polymerization algorithm for amorphous polymers. *Theor. Chem. Acc.* **132**, (2013).

33 Larsen, G. S., Lin, P., Hart, K. E. & Colina, C. M. Molecular Simulations of PIM-1-like Polymers of Intrinsic Microporosity. *Macromolecules* **44**, 6944-6951, (2011).

34 Srinivasan, R., Auvil, S. R. & Burban, P. M. Elucidating the mechanism(s) of gas-transport in poly 1-(trimethylsilyl)-1-propyne (PTMSP) membranes. *J. Membr. Sci.* **86**, 67-86, (1994).

35 Ichiraku, Y., Stern, S. A. & Nakagawa, T. An investigation of the high gas-permeability of poly (1-trimethylsilyl-1-propyne). *J. Membr. Sci.* **34**, 5-18, (1987).

36 Merkel, T. C., Bondar, V., Nagai, K. & Freeman, B. D. Sorption and transport of hydrocarbon and perfluorocarbon gases in poly(1-trimethylsilyl-1-propyne). *J. Polym. Sci., Part B: Polym. Phys.* **38**, 273-296, (2000).

37 Nakagawa, T., Saito, T., Asakawa, S. & Saitoh, Y. Polyacetylene derivatives as membranes for gas separation. *Gas Sep. Purif.* **2**, 3-8, (1988).

38 Robeson, L. M. The upper bound revisited. *J. Membr. Sci.* **320**, 390-400, (2008).

39 Jue, M. L., Breedveld, V. & RP, L. Defect-free PIM-1 hollow fiber membranes. *J. Membr. Sci.* **530**, 33-41, (2017).

40 Swaidan, R., Ghanem, B., Litwiller, E. & Pinnau, I. Physical Aging, Plasticization and Their Effects on Gas Permeation in "Rigid" Polymers of Intrinsic Microporosity. *Macromolecules* **48**, 6553-6561, (2015).

41 Nagai, K., Masuda, T., Nakagawa, T., Freeman, B. D. & Pinnau, I. Poly 1-(trimethylsilyl)-1-propyne and related polymers: synthesis, properties and functions. *Prog. Polym. Sci.* **26**, 721-798, (2001).

42 Merkel, T. C., Gupta, R. P., Turk, B. S. & Freeman, B. D. Mixed-gas permeation of syngas components in poly(dimethylsiloxane) and poly(1-trimethylsilyl-1-propyne) at elevated temperatures. *J. Membr. Sci.* **191**, 85-94, (2001).

43 Takada, K., Matsuya, H., Masuda, T. & Higashimura, T. Gas-permeability of polyacetylenes carrying substituents. *J. Appl. Polym. Sci.* **30**, 1605-1616, (1985).

44 Morliere, N., Vallieres, C., Perrin, L. & Roizard, D. Impact of thermal ageing on sorption and diffusion properties of PTMSP. *J. Membr. Sci.* **270**, 123-131, (2006).

45 Tsuchihara, K., Masuda, T. & Higashimura, T. Polymerization of silicon-containing diphenylacetylenes and high gas-permeability of the product polymers. *Macromolecules* **25**, 5816-5820, (1992).

46 Nguyen, P. T. *et al.* A dense membrane contactor for intensified CO2 gas/liquid absorption in post-combustion capture. *J. Membr. Sci.* **377**, 261-272, (2011).

47 Dibrov, G. A. *et al.* Robust high-permeance PTMSP composite membranes for CO2 membrane gas desorption at elevated temperatures and pressures. *J. Membr. Sci.* **470**, 439-450, (2014).

48 Pinnau, I. & Toy, L. G. Transport of organic vapors through poly(1-trimethylsilyl-1-propyne). *J. Membr. Sci.* **116**, 199-209, (1996).

49 Raharjo, R. D., Freeman, B. D., Paul, D. R. & Sanders, E. S. Pure and mixed gas CH4 and n-C4H10 permeability and diffusivity in poly(1-trimethylsilyl-1-propyne). *Polymer* **48**, 7329-7344, (2007).

50 Fadeev, A. G. *et al.* Extraction of butanol from aqueous solutions by pervaporation through poly(1-trimethylsilyl-1-propyne). *J. Membr. Sci.* **186**, 205-217, (2001).

Methods

Synthesis

Full details of all monomer synthesis and the preparation of polymers PIM-BTrip and PIM-TMN-Trip-TB are given in the Supplemental Information.

Synthesis of PIM-TMN-Trip.

Monomer TMN-Trip (2.34 g, 4.61 mmol) and tetrafluoroterephthalonitrile (0.92 g, 4.61 mmol) were dissolved in anhydrous DMF (40.0 mL). To this, anhydrous K_2CO_3 (5.09 g, 36.9 mmol) was added and the mixture heated to 65 °C for 96 h. The reaction mixture was poured into water, neutralised with dilute HCl solution and the solid collected by filtration then washed with water, acetone and methanol. The polymer was purified by repeated precipitation from $CHCl_3$ solution by dropping into a mixture of methanol: acetone (2:1). The purified polymer was collected by filtration and dried under vacuum at 100 °C to yield a yellow powder (1.95 g, 67 % based on the

molecular weight of the repeated unit); ν_{max} (cm^{-1}): 2924, 2239, 1740, 1607, 1435, 1385, 1269, 1155, 1005, 905, 883, 750, 669, 538; ^{1}H NMR (500 MHz, $CDCl_3$) δ (ppm) 7.66 (s, 2H), 7.56 (s, 2H), 6.96 (s, 4H), 2.37 (s, 6H), 1.70 (s, 4H), 1.31 (s, 12H); ^{13}C NMR (101 MHz, *solid state*) δ (ppm) 143.9, 138.7, 130.5, 124.7, 117.8, 109.1, 94.5, 47.6, 34.3, 12.9; BET surface area = 1034 $m^2\ g^{-1}$; total pore volume = 0.87 $cm^3\ g^{-1}$ at P/P_o = 0.98 from N_2 adsorption at 77 K; GPC ($CHCl_3$): M_n = 52,300 g mol^{-1}, M_w = 197,000 g mol^{-1}; TGA analysis (nitrogen): Initial weight loss due to thermal degradation commences at ~474 °C

Synthesis of PIM-TMN-SBI.

A mixture of monomer TMN-SBF (1.286 g, 2.1410 mmol) and 2,3,5,6-tetrafluoroterephthalonitrile (428 mg, 2.1410 mmol) in anhydrous DMF (25 mL) was stirred under a dry nitrogen atmosphere. The mixture was heated to 30 °C and anhydrous K_2CO_3 (2.36 g, 17.13 mmol) added. The temperature was then raised to 65 °C and the mixture stirred for 92 h. After cooling, the reaction was poured into water (150 mL), the precipitate filtered off and washed repeatedly with water and acetone and dried in a vacuum oven. The solid was purified by reprecipitation from $CHCl_3$ solution (60 mL), which was filtered through cotton wool then poured into a flask containing a mixture of acetone/methanol (2/1, 180 mL). The product was collected by filtration and dried under high vacuum overnight to give the final product as a yellow solid (1.320 g, 85% based on the molecular weight of the repeat unit); ν_{max} (cm^{-1}): 2959, 1445, 1400, 1364, 1263, 1171, 1144, 1010, 874, 748; ^{1}H NMR (500 MHz, $CDCl_3$) (ppm) 7.66 (br s, 1H), 7.43 (br s, 1H), 6.67 (br s, 1H), 6.32 (br m, 1H), 1.69 (br s, 4H), 1.42 (s, 6H), 1.07 (br m, 6H); ^{13}C NMR (101 MHz, *solid state*) δ (ppm) 145.5, 139.4, 117.5, 108.2, 95.5, 66.0, 34.6, 31.5; BET surface area = 1013 $m^2\ g^{-1}$; total pore volume = 0.93 $cm^3\ g^{-1}$ at P/P_0 = 0.98, from N_2 adsorption at 77 K; GPC ($CHCl_3$); M_n = 68,000 g mol^{-1}, M_w = 154,000 g mol^{-1}; TGA analysis (nitrogen): 1.0 % loss of weight occurred below 300 °C. Initial weight loss due to thermal degradation commences at ~465 °C.

Macromolecular packing simulation

PIM-TMN-Trip and PIM-TMN-SBI polymer frameworks were constructed using the Polymatic simulated polymerization algorithm[32] and the '21-step' compression/decompression scheme.[33] The polymatic simulated polymerization algorithm involves virtual polymerization through

artificially bonding adjacent chemical repeat units together in cycles along with molecular dynamics simulations to form long polymer chains. First, 500 repeat monomers of PIM-TMN-Trip or PIM-TMN-SBI were randomly packed into a simulation box under periodic boundary conditions at a low arbitrary density of 0.3−0.4 g/cm^3 following polymerization via Polymatic. In order to obtain the final simulation box at relevant experimental conditions, the '21-step' compression/decompression scheme was used.[33] During the polymerization steps, additional charges on 'reactive atoms' (q_{polym} = ±0.5e) were used to accelerate the polymerization process. During polymerization, 'reactive atoms' on neighboring monomers within a cutoff distance of 6 Å or less were bonded together.[32] The polymerization of neighboring monomers was carried out until no more bonds could be found within the specified cutoff distance for at least 500 ps following the compression/decompression scheme where T_{max} = 1000 K, P_{max} = 5 × 10^4 atm, T_{final} = 300 K, and P_{final} = 1 atm were employed according to previous work.[33] Pore size characterization, gas adsorption and gas permeability of both polymers were calculated from the simulation models as described in the Supplemental Information.

Physical Characterization

Gas adsorption and calculation of pore size distribution

The N_2 adsorption isotherms at 77 K were measured using a Quantachrome Autosorb iQ2. CO_2 (273 K) sorption data were acquired using a Quantachrome Autosorb iQ. The powder samples were degassed for 600 min at 120 ºC before the experiment. The adsorption isotherm was used to calculate the pore volume and the pore size distribution; the Horwath-Kawazoe (HK) model was applied considering the adsorbent geometry as carbon slit pores for all cases.

Wide-angle X-ray scattering (WAXS)

Wide-angle X-ray scattering (WAXS) analysis was performed in the reflection mode at room temperature by using a Bruker D8 Advance diffractometer fitted with a Goebel mirror and provided with a PSD Vantec detector. Cu Kα radiation source of wavelength 1.54 Å was used, operating in a 2θ range of 2–55° with a scan rate of 0.5 s per step.

Density measurement

The bulk density was measured for the MeOH treated sample after conditioning at 140°C. This should be the most representative sample, free from residual solvent and without too much excess free volume introduced by the swelling in MeOH. The bulk density was calculated from the mass per unit volume of three test specimens for the mechanical tests. The sample mass was measured with an analytical balance and the sample volume was determined from the length, width and average thickness of the tests strips, determined by a digital Micrometer (Mitutoyo).

Tensile tests

The mechanical properties of the membranes were determined by tensile tests at room temperature on a Zwick/Roell single column Universal Testing Machine, model Z2.5, equipped with a 200N load cell and flat grinded steel pneumatic clamps, covered with abrasive paper to avoid slip. Specimens with an effective length of 30 mm (distance between the clamps) and a width of 5 mm were tested at a deformation rate of 3 mm min^{-1} (= 10 % min^{-1}). The average value and the standard deviation of the Young's modulus, the tensile strength and the maximum deformation were determined on a series of 3 samples (Supplemental Fig. 9). The tests show excellent repeatability of the samples

Pure gas permeation

Pure gas permeation experiments were carried out on a custom made fixed-volume/pressure increase instrument constructed by Elektro & Elektronik Service Reuter (Geesthacht, Germany), equipped with a turbomolecular pump and a membrane-backing pump. In standard experiments, the feed gas pressure was regulated at 1 bar (the actual value was read with a resolution of 0.1 mbar); the permeate pressure was measured in the range from 0 to 13.3 mbar (maximum), with a resolution of 0.0001 mbar. The gases were generally tested in the same order (H_2, He, O_2, N_2, CH_4, and CO_2). Nevertheless, it was verified by repeating a measurement cycle, that the measurement order for these materials was irrelevant at a feed pressure of 1 bar, provided that sufficiently long vacuum was applied to completely remove the previous gas.

Feed pressure, permeate pressure, and temperature were continuously recorded during each measurement run. The temperature was controlled at a constant temperature of 25±1 °C. Before the first measurement, the membrane was evacuated for sufficient time inside the cell (at least 1 h). Between two subsequent measurements, the system was evacuated for a period of at least ten

times the time lag of the previous species in order to guarantee the complete removal of the previous gas. In repeated cycles, changes between the first and second cycle were generally much less than 5%. Circular membranes, with an effective exposed surface area of 2.14 cm^2 were used. Experimental details of mixed gas permeability, elevated temperature measurements and data fitting are given in the Supplemental Information.

Data Availability Statement.

The spectroscopic and gas permeability data that support the findings of this study are available from Edinburgh DataShare (http://datashare.is.ed.ac.uk) with the identifier http://dx.doi.org/10.7488/ds/2054. Data are also provided in the Supplemental Information, which is available in the online version of the paper. The crystallographic data for the monomers TMN-Trip and TMN-SBI can be obtained free of charge from the Cambridge Crystallographic Database (CCDC) under deposition numbers CCDC 1495014 and 1495015.

Corresponding author

Correspondence and requests for materials to neil.mckeown@ed.ac.uk

Acknowledgments:

The research leading to these results has received funding from the Horizon 2020/FP7 Framework Program under grant agreement n° 608490, project M^4CO_2 and from the EPSRC (UK) grant numbers EP/M01486X/1 and EP/K008102/2. This work was also supported by the US National Science Foundation (DMR-1604376) and the Leverhulme Trust, UK (RPG-2014-308). High-performance computational resources were provided by the University of Florida Research Computing and the Research Computing and Cyberinfrastructure unit at Pennsylvania State University.

Author contributions

I.R. prepared PIM-TMN-Trip, C.G.B prepared PIM-TMN-SBI and performed the crystallographic study of the monomers. M.C. prepared the films for gas permeability and coordinated the experimental part of the project. B.C.G verified the synthesis of PIM-TMN-Trip and performed the WAXS analysis. E. L. performed the high temperature gas permeability measurements. MCF performed the gas adsorption measurements and Horvath-Kawazoe analysis of pore size distribution and designed the high temperature gas permeability experiments. P.B.

designed and performed the film conditioning protocol and carried out the elaboration of the single gas permeability data to evaluate the transport parameters (Table 1: data series 1-5, 8-10). C.G. performed the single gas permeability measurements (Table 1: data series 1-5, 8-10), A.F. performed the single gas permeability measurements (Table 1: data series 6) and the elaboration of the data. J.C.J. performed the mixed gas experiments, the density and tensile strength analysis and supervised the gas permeability work and data elaboration. K.E.H devised the methodology for simulation and analysis of the chain packing of PIMs related to PIM-TMN-SBI. T.P.L.A. performed the simulation and analysis of the chain packing of PIM-TMN-Trip. C.M.C. designed and supervised the chain packing simulation work. N.B.M designed the polymers and prepared the manuscript with input from all of the other authors.

Competing financial interests

The authors declare no competing financial interests.

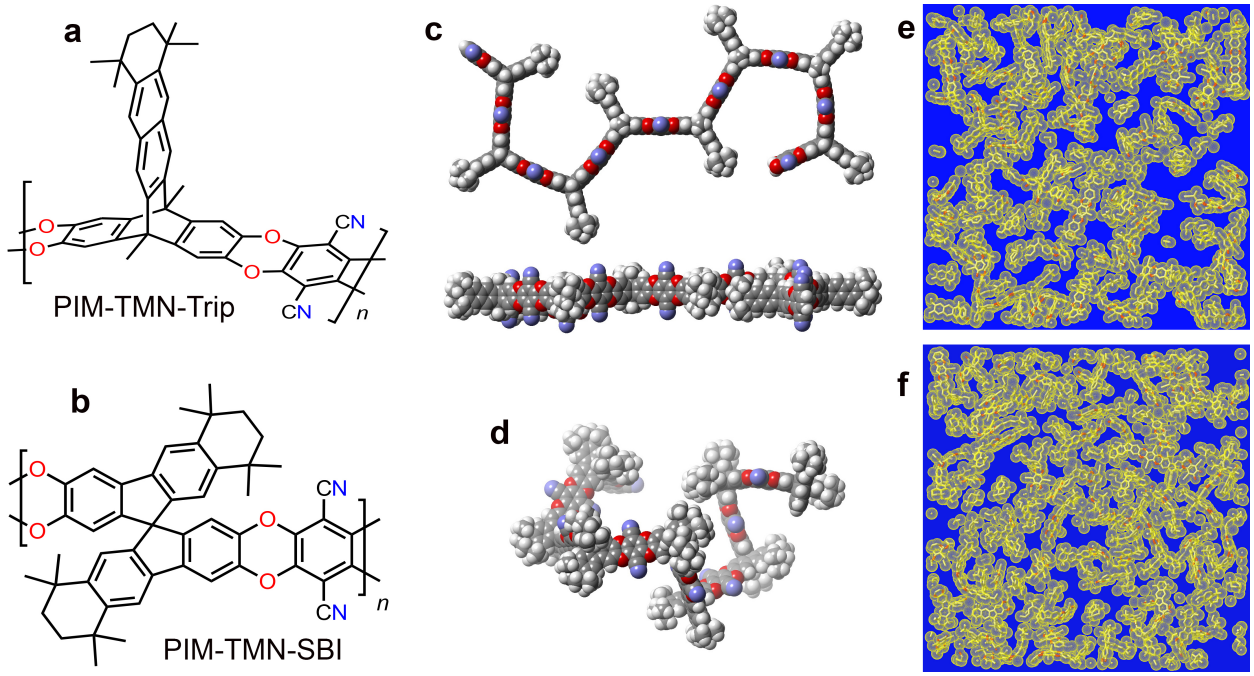

Figure 1. A comparison of the macromolecular chain structures of PIM-TMN-Trip and PIM-TMN-SBI and their packing. a Molecular structures of PIM-TMN-Trip and **b.** PIM-TMN-SBI. **c.** Two views of the energy-minimized 2-D shape of a chain fragment of PIM-TMN-Trip containing 16 monomeric units and **d.** The analogous 3-D conformation of a chain fragment of PIM-TMN-SBI. **e.** Structure of a 1 nm thick cross-section of the 9 × 9 × 9 nm sample of the simulated packing of 2D PIM-TMN-Trip with the van der Waals surface of the polymer chains shaded yellow and the free volume shaded blue. The amount of free volume (i.e. microporosity) is larger than in the analogous packing structure of 3D PIM-TMN-SBI shown in **f.**

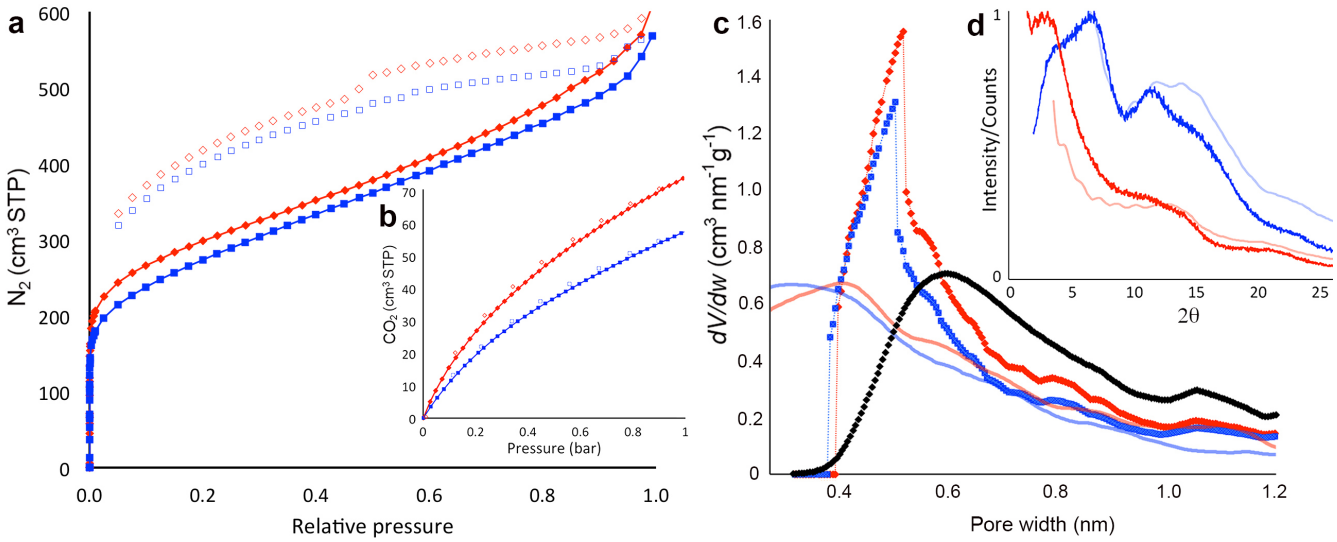

Figure 2. Data from the physical characterization of PIM-TMN-Trip (red) and PIM-TMN-SBI (blue). (**a**). N_2 adsorption and desorption isotherms at 77 K. (**b**) CO_2 adsorption and desorption isotherms at 273 K. (**c**) Apparent pore-size distribution (PSD) calculated from low pressure N_2 adsorption data using the Horvath-Kawazoe method with the PSD for PTMSP shown in black.[12] The PSD calculated from the packing models of PIM-TMN-Trip and PIM-TMN-SBI is shown in a lighter shade of red/blue, respectively. The discrepancy between experimental and simulated data for smaller pore sizes is mainly due to the restricted access of the N_2 probe (kinetic diameter = 0.37 nm) into smaller pores, which contribute collectively to the maxima at pore width = 0.5 nm. (**d**) Wide-angle-x-ray-scattering (WAXS) data from cast films plotted with simulated data from the packing models, which are shown in a lighter shade of red/blue for PIM-TMN-Trip and PIM-TMN-SBI, respectively. It should be noted that the calculated scattering from the simulated packing loses precision at values of $2\theta < 5°$ due to the finite size of the model samples (~9 × 9 × 9 nm).

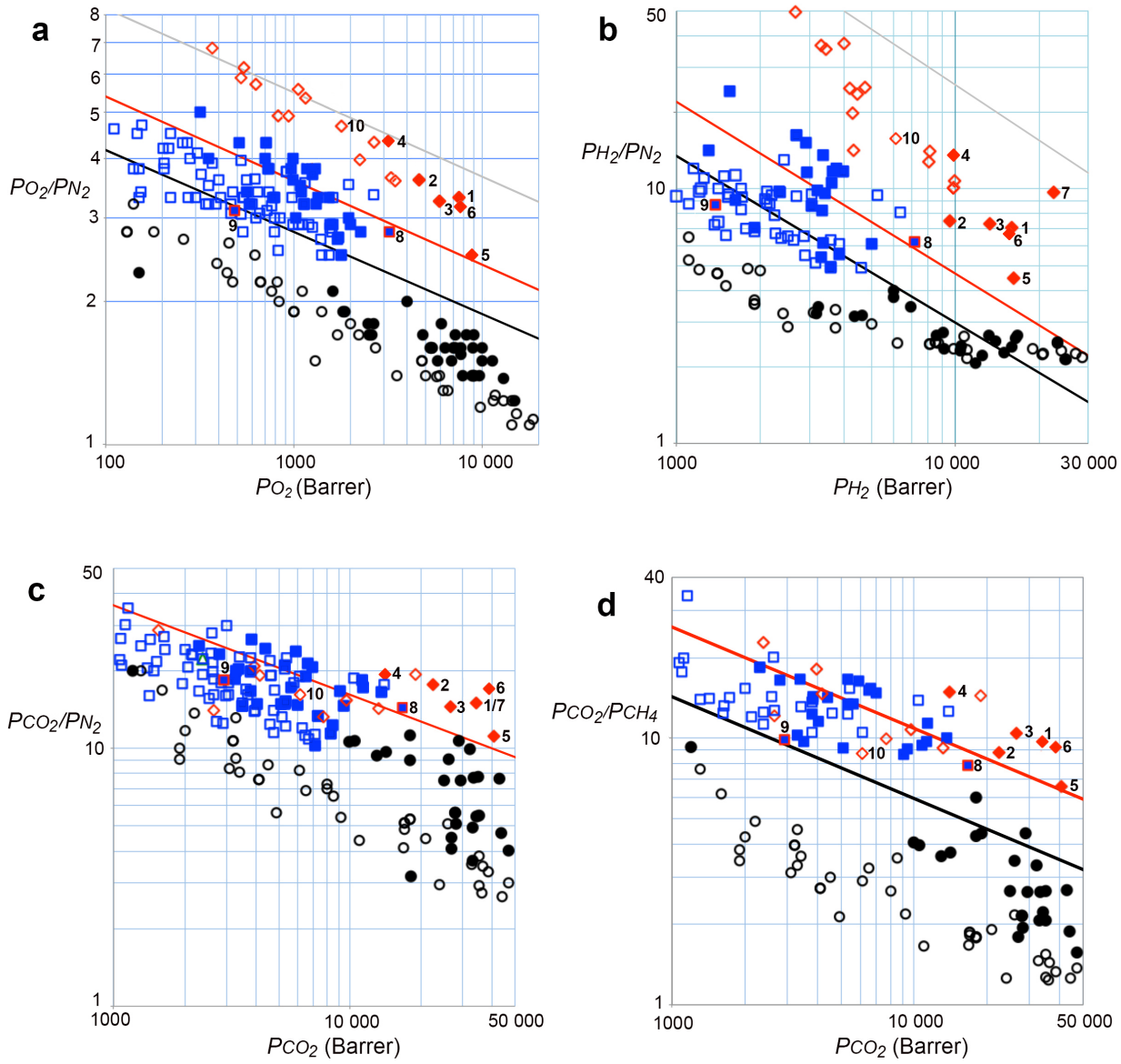

Figure 3. Robeson Plots for (A) O_2/N_2, (B) H_2/N_2, (C) CO_2/N_2 and (D) CO_2/CH_4 with the 1991 upper bounds indicated by a black line, 2008 by a red line and those proposed for 2015 by gray lines. Filled red diamonds show the data for PIM-TMN-Trip and red-trimmed blue-filled squares show the data for PIM-TMN-SBI with the accompanying numbers indicating the film history (See Table 1). Accumulated literature data for triptycene and other bridged bicyclic based PIMs (red open diamonds); PIM-1 (filled blue squares); other spirobisindan-based PIMs (open blue squares); PTMSP (filled black circles) and other polyacetylenes (open black circles) are shown for comparison.

Table 1 Gas permeability values (P_x, Barrers) and selectivities (P_x/P_{N_2}) for PIM-TMN-Trip, PIM-TMN-SBI and PIM-TMN-Trip-TB measured from films with different processing histories.

Polymer	Film history	P_{He} (P_{He}/P_{N_2})	P_{H_2} (P_{H_2}/P_{N_2})	P_{O_2} (P_{O_2}/P_{N_2})	P_{CO_2} (P_{CO_2}/P_{N_2})	P_{N_2}	P_{CH_4} (P_{CH_4}/P_{N_2})
PIM-TMN-Trip	1	6370	16900	7470	33300	2230	3420
		(2.86)	(7.58)	(3.35)	(14.9)		(1.53)
	2	3560	9590	4600	22500	1270	2470
		(2.80)	(7.53)	(3.61)	(17.7)		(1.94)
	3	4880	13400	5950	27000	1830	2590
		(2.66)	(7.32)	(3.25)	(14.7)		(1.41)
	4	3930	9840	3160	14100	727	943
		(5.41)	(13.5)	(4.35)	(19.3)		(1.30)
	5	5820	16300	8780	40700	3530	6070
		(1.65)	(4.62)	(2.49)	(11.5)		(1.72)
	6	5720 ±340	15800 ±940	7520 ±570	38400 ±2970	2340	4230 ±460
		(2.45±0.08)	(6.79±0.23)	(3.22±0.06)	(16.4±0.27)	±211	(1.81± 0.04)
	7	4520	22600		34400	2350	
		(1.90)	(9.70)		(14.6)		
	7a		19700		48400	3510	
			(6.10)		(15.0)		
	Model	3840	36200	6360	48800	2720	6190
		(1.40)	(13.3)	(2.30)	(17.9)		(2.30)
PIM-TMN-SBI	8	2720	7190	32001	17500	1080	2100
		(2.51)	(6.65)	(2.96)	(16.2)		(1.95)
	9	646	1370	485	2980	160	300
		(4.04)	(8.58)	(3.04)	(18.7)		(1.89)
	Model	1840	8510	1620	10000	558	1070
		(3.30)	(15.2)	(2.90)	(17.9)		(1.90)
PIM-TMN-Trip-TB	10	2300	6100	2030	6060	396	710
		(5.80)	(15.4)	(5.13)	(15.3)		(1.80)

1. Methanol treated 195 μm thick film; 2. Methanol treated 192 μm thick film aged 39 days; 3. Methanol treated 193 μm thick film heated at 120 °C for 24 h then aged for 14 days; 4. Aged film 187 μm thick film heated at 120 °C for 24 h then aged for 365 days; 5. Aged 195 μm thick film after second methanol treatment; 6. Average values ± standard deviation of 4 samples: methanol treated 156±5 μm thick films and subsequently heated at 140 °C for 4 h; 7. Methanol treated 60 μm thick film; 7a. Film as for 7 but data collected at 93-100 °C. 8. Methanol treated 166 μm thick film, 9. Methanol treated 110 μm thick film heated at 120 °C for 24 h then aged for 14 days. 10. Methanol treated 125 μm thick film of PIM-TMN-Trip-TB, for which the molecular structure is shown in Supplementary Fig. 1. Note that 1-6, 8, 8-10 measured at ITM, 7 and 7a measured at University of Edinburgh.